applied sciences

MDPI

Article

Calculation of Heat Transfer and Drag Coefficients for Aircraft Geometric Models

Victor V. Kuzenov [1], Sergei V. Ryzhkov [1,*] and Aleksey Yu. Varaksin [2]

[1] Thermal Physics Department, Bauman Moscow State Technical University, 105005 Moscow, Russia
[2] Joint Institute for High Temperatures, Russian Academy of Sciences, 125412 Moscow, Russia
* Correspondence: svryzhkov@bmstu.ru; Tel.: +7-(499)-263-6570

Abstract: A numerical model to calculate the heat transfer and resistance coefficients near the bodies of complex geometric shapes moving at high velocity is formulated. The processes of heat and mass transfer and flow around aircraft elements are considered. An algorithm for calculating heat fluxes and the heat transfer coefficient is proposed. The developed numerical technique can give an idea of the essential features of the flow, heat transfer at the end keels of the wings, and integral layouts of high-speed aircraft. An approximate mathematical model for calculating the heat transfer processes and resistance coefficients near the bodies of complex geometric shapes moving at high speed in the Earth's atmosphere is formulated. The calculated results for convective heat transfer and friction coefficients for the X-33 and X-43 vehicles are obtained.

Keywords: aerodynamic computation; convective heat transfer; high-speed aircraft; turbulent boundary layer; aerospace

check for updates

Citation: Kuzenov, V.V.; Ryzhkov, S.V.; Varaksin, A.Y. Calculation of Heat Transfer and Drag Coefficients for Aircraft Geometric Models. *Appl. Sci.* **2022**, *12*, 11011. https://doi.org/10.3390/app122111011

Academic Editors: Ignazio Dimino and Cristian Vendittozzi

Received: 5 September 2022
Accepted: 27 October 2022
Published: 30 October 2022

Publisher's Note: MDPI stays neutral with regard to jurisdictional claims in published maps and institutional affiliations.

Copyright: © 2022 by the authors. Licensee MDPI, Basel, Switzerland. This article is an open access article distributed under the terms and conditions of the Creative Commons Attribution (CC BY) license (https://creativecommons.org/licenses/by/4.0/).

1. Introduction

The design of new aerospace aircraft (including those designed for cruising flight within the Earth's atmosphere) for aerospace purposes requires the fundamental experimental and theoretical calculations of aerodynamic characteristics, heat and mass transfer processes, and features of flow around integral assemblies of high-speed aircraft. It should be noted that knowledge of the aerodynamic coefficients makes it possible to calculate the trajectory of a high-speed aircraft in the Earth's atmosphere, as well as validate the computational codes being developed. Experimental studies in this case are expensive, and in many cases (underground conditions) modeling the physicochemical processes accompanying high-speed aircraft (HSA) flights is fundamentally impossible.

At the same time, the object of numerical research can be simplified (for example, a schematized shape of the keel, wing, and nose of the HSA), and a computer model of a high-speed aircraft close to the real one, designed taking into account the general principles of the integration of aerospace objects. The calculation of the fields of gas-dynamic parameters for a time-averaged flow also makes it possible to study the transition to the turbulent regime of airflow in the boundary layer, the stability of which is very sensitive to changes in flow characteristics.

To obtain a sufficiently high lift-to-drag ratio, it is also noted that the HSA should not have significant resistance, in particular, its supporting and stabilizing organs should be thin. However, in order to be able to remove a sufficiently large amount of heat from the leading edges of the wings and keel, these edges must be blunted. In this case, the absorption effect of the entropy layer by the boundary layer is of interest, which occurs when flowing around blunt bodies. This effect can be singled out as the main effect of all the second-order effects of the boundary layer theory.

Thus, an important practical element of such research is the search for ways to reduce heat fluxes and drag, as well as stabilize the flight of HSA when high-speed aircraft are moving in the range of trans- and supersonic speeds. In addition, knowledge of the aerodynamic coefficients in a wide range of Mach numbers and angles of attack makes it possible to calculate the trajectory of a high-speed aircraft in the Earth's atmosphere, as well as to validate the developed computational codes.

Many physical problems arise when designing HSA integrated circuits. For example, the flow of gas (plasma) in the shock layer is complicated due to the development of several phenomena specific to HSA.

First, the flows behind intense shock waves are very inhomogeneous and contain sharp gradients of vorticity, pressure, temperature, entropy, etc. The interaction of these subregions (entropy and vortex layers) with a viscous boundary layer significantly affects the heat transfer and frictional resistance to HSA motion.

Secondly, at high speeds and flight altitudes, the air in the shock layer can no longer be considered a perfect gas, and its real properties must be taken into account. At the same time, at the Mach number, the shock layer is strongly compressed due to intense plasma–chemical reactions (mainly due to nonequilibrium reactions of dissociation, recombination, and ionization of molecules in a compressed and chemically active boundary layer), leading to a decrease in the effective adiabatic exponent.

Thirdly, it is necessary to evaluate the effect of the possibility of cooling the surface of the wings, keel, and body of the HSA on the flow characteristics in a laminar boundary layer flown by a high-speed viscous gas (plasma) flow in the regime of strong viscous–inviscid interaction.

Fourthly, at high angles of attack, the central keel (such an arrangement of the keel facilitates the solution of the problem of its thermal protection), streamlined by a detached stream of rarefied air, is ineffective and is used for stabilization and control purposes only at the end of the descent trajectory, when the flight passes at a low angle of attack. In this case, the use of end keels is often envisaged (the numerical technique proposed in this paper allows one to study heat transfer on the surface of the end keel and in the zone of its interface with the wing), which are effective both at low and at high angles of attack.

A lot of physical problems arise when developing HSA [1–9], of which we single out the following two (this paper is devoted to these problems): the calculation of viscous shear stresses (and coefficient of friction C_f) on an aircraft surface and heat flow $q_{w,L}$. The direct way to quickly estimate the friction coefficient and heat fluxes by numerically integrating the complete system of Navier–Stokes equations is problematic. This is because the size of the body (about ten meters) is much larger than the characteristic size of the boundary layer (about 1 mm), and the need to resolve the boundary layer near the surface of the streamlined body leads to the fact that the computational grid will require large sizes of random access memory (RAM).

Therefore, one of the objectives of the research is to develop a simplified (operational) method for assessing convective heat fluxes and drag coefficients for bodies of complex spatial shapes. The estimation (based on the simplified method) of heat fluxes and drag coefficients should be preceded by the calculation, using the Euler equations.

Focusing on the related achievements that are used as reference data [10,11] for the proposed work, [10] provides an overview of hypersonic computational fluid dynamics research conducted at the NASA Langley Research Center to support the Phase II development of the X-33 vehicle. The X-33, which is being developed by Lockheed Martin in partnership with NASA, is an experimental single-stage-to-orbit demonstrator that is intended to validate critical technologies for a full-scale reusable launch vehicle. Laminar and turbulent predictions were generated for the X-33 vehicle using two finite-volume Navier–Stokes solvers. Inviscid solutions were also generated with an Euler code. Computations were performed for Mach numbers from 4.0 to 10.0, at angles of attack from 10 deg to 48 deg, with body flap deflections of 0, 10, and 20 deg. Comparisons between predictions and wind tunnel aerodynamic and aero-heating data are presented in this paper.

In paper [11], computer modeling of the aerodynamic coefficients of a model of a high-speed aircraft similar to the X-43, moving with a Mach number M = 7, was performed. Devices with arbitrary geometry in three-dimensional unstructured tetrahedral meshes. A cross-verification of these computer codes was carried out based on a comparison of the distributions of aerodynamic parameters, and values of aerodynamic characteristics. It is shown that these computer codes give a fairly reliable picture of the distribution of the fields of the sought values, and also calculate the aerodynamic characteristics with high accuracy relative to each other.

2. Mathematical Model for Assessing Convective Heat Fluxes near the Surface of Bodies of a Simple Geometric Shape

This section provides a brief 2D description of an approximate method for estimating heat fluxes in key elements (hull and wing edges, nose fairing, etc.,) of an aircraft that have the simplest spatial forms, for example, in the form of a sphere or a wedge associated with a cylinder, etc. Note that in the situation under consideration, compressed and heated (in a shock wave) to a high temperature (>1000 K), air convectively transfers energy into the wall material of the HSA head. This energy is further redistributed along the walls of the working compartment of the HSA. At the same time, it is in the key elements and the head part that the wall material experiences the maximum thermal load.

In the general case, to solve such a problem it is necessary to carry out a computational–theoretical study of the features of the structure and the spatial distributions of the gas-dynamic parameters of the flow near the HSA surface, and, based on this study, evaluate the convective heat fluxes.

It follows from the formulas below that the heat transfer coefficient at the critical point is inversely proportional to the square root (proportional in the turbulent case) of the blunt radius. Therefore, at high flight speeds and, accordingly, high stagnation temperatures, with a decrease in the bluntness radius at the critical point, the values of convective and radiative fluxes, as well as the magnitudes of thermal deformations, sharply increase (i.e., the geometric shape of the streamlined body changes).

The mathematical relationships of the 2D model follow from the relationships of the 3D model. The mathematical model of thermophysical processes that occur when flowing around bodies of simple geometric shapes is based on multicomponent Euler radiation equations. Note that the calculation of heat fluxes in the case under consideration is always preceded by the determination of an external inviscid flow near the surface of the streamlined body. Calculations of this kind were performed using the 2D Euler radiation equations and using a nonlinear quasi-monotone compact-polynomial difference scheme [3,12]. The calculation of the optical parameters of the working media included in this system of equations was carried out using the ASTEROID computer system [13].

3. Mathematical Model for Calculating Convective Heat Fluxes for HSA of Complex Spatial Shape

In references [3,14], a version of the effective length method is proposed, which allows the finding of the different coefficients. The area of applicability of the effective length method is of the flows at relatively large Reynolds numbers (Re > $10^4 \div 10^5$). This approximate method is applicable only in flow regions with low-pressure gradients along the streamline and in the absence of separation zones.

The effective length is determined on the HSA surface (here the symbol denotes the length of the curve along the streamline) as:

$$\ell_{eff} = \frac{\int\limits_0^x \left[\Pi^2 K^2 K_1^2 \mu_0 \rho_0 U_0 C_{p,0}^2 (T_e - T_w)^2 Pr_0^{-4/3}\right] \mathrm{d}s}{\left[\Pi^2 K^2 K_1^2 \mu_0 \rho_0 U_0 C_{p,0}^2 (T_e - T_w)^2 Pr_0^{-4/3}\right]} \quad (1)$$

Under the integral are the variables varying from the beginning of the formation of the boundary layer (the critical point is the stagnation point of the flow incident on the HSA) to the considered section.

The integrand values are variables that vary from the beginning of the formation of the boundary layer (the critical point–braking point flux incident on the HSA) before the section under consideration, where $\Pi = R_{ef}(s)$ is the metric coefficient and average radius of curvature (for a non-axisymmetric body), respectively, determined and serving to take into account the increase or decrease in the thickness of the boundary layer due to runoff or spreading of streamlines; $\mu_0, \rho_0, U_0, M_0, Pr_0$—dynamic viscosity coefficient, density, velocity, local Mach, and Prandtl number, respectively, taken at the outer edge of the boundary layer, at the point coordinate of the current line; T_w, T_e are the body temperature and wall temperature, respectively:

$$T_e = T_0\left(1 + r\frac{\gamma - 1}{2}M_0^2\right), \quad r = \sqrt{Pr_0} \tag{2}$$

where r is the recovery factor.

K_1 and K (effect of compressibility) are introduced as:

$$K_1 = \left[1 + 0.16\left(1 + \frac{T_w}{T_0^*}\right)\left(\frac{2m}{m+1}\right)^{1/3}\right]^{1/2} \tag{3}$$

$$K = \left(\frac{\rho_0\mu_0}{\rho_w\mu_w}\right)^{1/3} \tag{4}$$

The dimensionless velocity gradient can be expressed as:

$$m = \frac{x}{V_0}\frac{\partial V_0}{\partial x} \tag{5}$$

The Reynolds and Stanton numbers are determined as:

$$St_{eff} = 0.332(m+1)^{1/2}\mathrm{Re}_{eff}^{1/2}\mathrm{Pr}_0^{-2/3}K \cdot K_1 \tag{6}$$

$$\mathrm{Re}_{eff} = \frac{\rho_w V_0 \ell_{eff}}{\mu_w} \tag{7}$$

Convective heat can be found as follows:

$$q_{w,L} = (C_p)_{cp}^*\rho_0 V_0(T_e - T_w)St_{eff} \tag{8}$$

The effective length for the turbulent regime can be obtained as follows:

$$\ell_{eff} = \frac{\int_0^x \left[\left[\Pi^{5/4}\left(1 + r\frac{\gamma-1}{2}M_0^2\right)^{0.1375}\rho_0 U_0 \mathrm{Pr}_0^{-0.7125}\mu_0^{0.25}C_{p,0}^{1.25}\right](T_w/T_e)^{0.5}(T_e - T_w)^{1.25}\right]\mathrm{d}s}{\left[\left[\Pi^{5/4}\left(1 + r\frac{\gamma-1}{2}M_0^2\right)^{0.1375}\rho_0 U_0 \mathrm{Pr}_0^{-0.7125}\mu_0^{0.25}C_{p,0}^{1.25}\right](T_w/T_e)^{0.5}(T_e - T_w)^{1.25}\right]} \tag{9}$$

where $r = \sqrt[3]{\mathrm{Pr}_0}$, and the heat flux is determined as follows:

$$q_{w,L} = (C_p)_{cp}^*\rho_0 V_0(T_e - T_w)St_{eff},\ \mathrm{Re}_{eff} = \frac{\rho_w V_0 \ell_{eff}}{\mu_w} \tag{10}$$

In Equations (1) and (9), the parameter Π, in the case of plane flow, $\Pi = R_{ef} = 1$, and for the cylindrical case in Equation (1), $\Pi^2 = R_{ef}^2$, and in Equation (9), $\Pi^{5/4} = R_{ef}^{5/4}$.

The Stanton number is written as follows:

$$St_{eff} = 0.0296\frac{1}{\mathrm{Re}_{eff}^{0.2}}\mathrm{Pr}_0^{-0.57}\left(\frac{T_w}{T_e}\right)^{0.4}\left(1 + r\frac{\gamma - 1}{2}M_0^2\right)^{0.11} \tag{11}$$

$\mathrm{Re}_{eff} = 10^5 \div 10^6$ or our flow conditions [15].

A fairly accurate way to describe the thermodynamic properties of individual chemical components is the approximation by polynomials of the form [16]:

$$\Phi_j = \varphi_{1,j} + \varphi_{2,j} \ln x + \varphi_{3,j} x^{-2} + \varphi_{4,j} x^{-1} + \varphi_{5,j} x + \varphi_{6,j} x^2 + \varphi_{7,j} x^3$$

$$\left(\frac{\mathrm{d}\Phi}{\mathrm{d}x}\right)_j = \left(\varphi_{2,j} - 2\varphi_{3,j} x^{-2} - \varphi_{4,j} x^{-1} + \varphi_{5,j} x + 2\varphi_{6,j} x^2 + 3\varphi_{7,j} x^3\right)\frac{1}{x}$$

$$\left(\frac{\mathrm{d}^2\Phi}{\mathrm{d}x^2}\right)_j = \left(-\varphi_{2,j} + 6\varphi_{3,j} x^{-2} + 2\varphi_{4,j} x^{-1} + 2\varphi_{6,j} x^2 + 6\varphi_{7,j} x^3\right)\frac{1}{x^2}$$

$$h_j = xT\left(\frac{\mathrm{d}\Phi}{\mathrm{d}x}\right)_j + \varphi_{8,j} \times 10^3, \text{ J/mol},$$

$$c_{p,j} = 2x\left(\frac{d\Phi}{dx}\right)_j + x^2\left(\frac{d^2\Phi}{dx^2}\right)_j, \text{ J/mol},$$

where $P_0 = 101325$, and Pa, $x = T \times 10^{-4}$ K. Approximation constants in the temperature range 298–20,000 K are presented in [17]. The reduced Gibbs energy is the number of chemical components of the gas mixture, the mass fraction of the i-th component of the mixture, and the specific heat capacity at constant pressure, enthalpy, and density of the i-th component of the mixture.

When calculating flow parameters with high Mach numbers and at high altitudes, the properties of equilibrium dissociating and chemically nonequilibrium air should be taken into account [18]. In such a gas, both molecular dissociation reactions and recombination reactions are realized. The presence of these reactions changes the mechanism of heat and mass transfer in the boundary layer, i.e., the processes of heat and mass transfer between the gas flow and the surface of the body are intensified. The level of the Mach criterion (M), at which these processes are realized in the compressed and boundary layers, determines the gas-dynamic nature of the flow, transferring it from supersonic to hypersonic. The beginning of such a transition corresponds to a flow with a value of $\mathrm{M} \geq 10$. From the point of view of heat fluxes and ballistics, in this case, calculations of a free molecular flow, and a transitional regime, both laminar and turbulent regimes are necessary. Note that in this case, it is preferable to use a different formulation of the thermodynamic model, separating the translational, electronic, vibrational, and rotational components of the total and internal energy, that is, using the Born–Oppenheimer approximation or the model of chemical kinetics, as described in [17].

Note that in the practical use of these relationships, it is necessary to be able to calculate with the required degree of accuracy, an integral $\int_0^S \rho^* \mu^* |V| r^2 \mathrm{d}s$ for the laminar flow and $\int_0^S \rho^* (\mu^*)^m |V| r^{c_3} \mathrm{d}s$ for the turbulent flow, where s is the distance along the streamline; r is the distance along the streamline in the direction of flow on the surface of the streamlined body; the distance along the current line in the flow direction on the body surface is the distance (axisymmetric case) from the axis x to a point on a streamlined body or the metric coefficient [19]. The calculation of these integrals makes it possible to find the thicknesses of the impulse loss g_L, and g_T, which have zero value at the stagnation point and which increase along the length of the aircraft (assuming that the calculation is carried out from the stagnation point).

Instead of direct calculation, for an arbitrary facet placed in a viscous turbulent flow, the local friction coefficient can be found using the general approximating dependence proposed in [20]:

$$C_f = C_{f0}\left(1 + r\frac{\gamma - 1}{2} M_0^2\right)^{-0.55}, \ r = \sqrt[3]{\mathrm{Pr}_0} \tag{12}$$

where $\gamma = \frac{C_p}{C_V}$ is the ratio of specific heat capacities; $M_0 = \frac{V_0}{a_0}$ ratio of specific heat capacities; is the local Mach number on the streamlined body, V_0, a_0 are the flow and sound velocities.

For the laminar case, the evaluation procedure is carried out as follows:

$$C_f = C_{f0}\left(1 + 0.72r\frac{\gamma - 1}{2}M_0^2\right)^{-0.15},\ C_{f0} = 0.646\mathrm{Re}_{eff}^{-0.5},\ r = \sqrt{\mathrm{Pr}_0} \tag{13}$$

After finding the local coefficient of friction at each point on the HSA surface $C_f = \frac{\left|\vec{V}\right|\tau_w}{\rho_\infty V_\infty^2/2}$, the total coefficients of friction C_{fx}, C_{fy} have the form:

$$\begin{aligned} C_{fx} &= \frac{1}{S_{mid}}\iint\limits_S \frac{\left(\vec{V}e_x\right)}{\left|\vec{V}\right|}\left(\frac{\left|\vec{V}\right|\tau_w}{\rho_\infty V_\infty^2/2}\right)\mathrm{d}S = \frac{1}{S_{mid}}\iint\limits_S \frac{\left(\vec{V}e_x\right)}{\left|\vec{V}\right|}C_f\mathrm{d}S, \\ C_{fy} &= \frac{1}{S_{mid}}\iint\limits_S \frac{\left(\vec{V}e_y\right)}{\left|\vec{V}\right|}\left(\frac{\left|\vec{V}\right|\tau_w}{\rho_\infty V_\infty^2/2}\right)\mathrm{d}S = \frac{1}{S_{mid}}\iint\limits_S \frac{\left(\vec{V}e_y\right)}{\left|\vec{V}\right|}C_f\mathrm{d}S \end{aligned} \tag{14}$$

The C_{f0} of in the turbulent case can be calculated using a number of empirical dependences, for example, $C_{f0} = 0.059\ \mathrm{Re}_{eff}^{-0,2}$, $\mathrm{Re}_{eff} = \rho_0 V_0 \ell_{eff}/\mu_0$. This dependence gives the most acceptable results in the considered range of Mach numbers, which is confirmed by numerous calculations.

It is most widespread when used in the range of Reynolds number from 10^6 to 10^8.

For the range of Reynolds numbers from 10^5 to 10^{10}, various simple formulas can be used to determine the local coefficient of friction, C_{f0}, depending on the local Reynolds number:

$$\begin{gathered} 10^5 \le \mathrm{Re}_{eff} \le 10^6;\ C_{f0} = 0.042\mathrm{Re}_{eff}^{-0.18},\ 10^6 \le \mathrm{Re}_{eff} \le 10^7;\ C_{f0} = 0.0322\mathrm{Re}_{eff}^{-0.16} \\ 10^7 \le \mathrm{Re}_{eff} \le 10^8;\ C_{f0} = 0,023\mathrm{Re}_{eff}^{-0,14} \\ 10^8 \le \mathrm{Re}_{eff} \le 10^9;\ C_{f0} = 0.016\mathrm{Re}_{eff}^{-0.12},\ 10^9 \le \mathrm{Re}_{eff} \le 10^{10};\ C_{f0} = 0.011\mathrm{Re}_{eff}^{-0.1} \end{gathered} \tag{15}$$

Using this approach in some cases allows you to get a more accurate result.

In addition to estimating the coefficient of friction drag on the body, within the framework of the approximate semi-empirical approach presented above, it is possible to determine at each specific point the characteristic parameters of the boundary layer (BL), such as BL thickness δ and integral thicknesses of BL—the displacement thickness δ * and the thickness of the momentum loss δ **. The displacement thickness δ * is a measure of the decrease in flow through the section due to the velocity decrease. The thickness of the momentum loss δ ** characterizes the decrease in the momentum in the section due to the deceleration of the flow.

A scheme for computing the characteristic boundary layer thickness at the point on the body in the case of a turbulent boundary layer is as follows: for each point of the body, the effective length is calculated; the calculated ℓ_{eff} determines the effective Reynolds number; further, for the incompressible case, the thickness δ, displacement thickness δ *, and momentum loss thickness δ ** are determined as follows: $\delta_H = 0,37 \cdot \ell_{eff} \cdot \mathrm{Re}_{eff}^{-0,2}$, $\delta_H^* = 0,125\ \delta_H$, $\delta_H^{**} = 0,097\ \delta_H$; after their determination, the characteristic thicknesses (compressible layer) are calculated using the following relations:

$$\begin{gathered} \delta_{\text{Сж}} = \delta_H\left(1 + 0.72r\tfrac{\gamma-1}{2}M_0^2\right)^{0.34},\ \delta_{\text{Сж}}^* = \delta_H^*\left(1 + 0.72r\tfrac{\gamma-1}{2}M_0^2\right)^{0.34} \\ \delta_{\text{Сж}}^{**} = \delta_H^{**}\left(1 + 0.72r\tfrac{\gamma-1}{2}M_0^2\right)^{-0.66},\ r = \sqrt[3]{\mathrm{Pr}_0} \end{gathered}$$

For the case of a laminar flow, a similar approach is used with the replacement of the corresponding relationships: first, for the incompressible laminar BL, the quantities δ_H, δ_H^*,

δ_H^{**}: $\delta_H = 4.64 \cdot \ell_{eff} \cdot \mathrm{Re}_{eff}^{-0.5}$, $\delta_H^{*} = 0.376\,\delta_H$, $\delta_H^{**} = 0.14\,\delta_H$ [21], then a set of characteristic thicknesses in compressible gas flow:

$$\delta_{Cж} = \delta_H \left(1 + 0.72 r \tfrac{\gamma-1}{2} M_0^2\right)^{0.85},\ r = \sqrt{Pr_0},\ \delta_{Cж}^{*} = \delta_H^{*}\left(1 + 0.72 r \tfrac{\gamma-1}{2} M_0^2\right)^{0.85},$$
$$\delta_{Cж}^{**} = \delta_H^{**}\left(1 + 0.72 r \tfrac{\gamma-1}{2} M_0^2\right)^{-0.15}$$

4. Results and Discussion

Only the main points of the computational algorithm for calculating aerodynamic heating and the friction coefficient are given here. A more detailed description can be found in the references [3,14].

In this work, a calculation technology based on an unstructured surface mesh was used to estimate heat fluxes and drag coefficients [22–25]. The calculation of the integrals included in expressions (1)–(16) requires finding the metric coefficients (local mean radius of curvature) included in the integrand.

In this case, when the aircraft surface is locally specified, the calculation of the local mean radius of curvature R_{ef} is based on the following symmetric form [19]:

$$K = \frac{1}{2}\frac{\left(1+f_u^2\right)f_{vv} - 2 f_u f_v f_{uv} + \left(1+f_v^2\right)f_{uu}}{\left(1+f_u^2+f_v^2\right)^{3/2}},\ R_{ef} = \frac{1}{K} \tag{16}$$

The partial derivatives $f_u, f_v, f_{uv}, f_{uu}, f_{vv}$ included in this relationship are:

$$\begin{gathered} f(u,v) \approx f\left(u_j, v_j\right) + f_u\left(u-u_j\right) + f_v\left(v-v_j\right) + \\ + f_{uu}\frac{\left(u-u_j\right)^2}{2} + f_{uv}\left(u-u_j\right)\left(v-v_j\right) + f_{vv}\frac{\left(v-v_j\right)^2}{2}. \end{gathered} \tag{17}$$

The calculation of an external inviscid flow (based on the Euler equations) near the surface of a streamlined body was performed using unstructured grids and the computational code from [17].

It is also noted that in the practical use of the developed methodology, it is necessary to be able to calculate the integrals of the form with the required degree of accuracy (above 2nd): $\int_0^S \rho^* \mu^* |V| r^2 ds$—for the laminar flow; $\int_0^S \rho^* (\mu^*)^m |V| r^{c_3} ds$, for the turbulent flow, where s is the distance along the streamline in the direction of flow on the surface of the streamlined body; r is the distance (for the axisymmetric case) from the axis Ox to a point $s(x,y,z)$ on the surface of the streamlined body $F(x,y,z)$, or the metric coefficient (the local average curvature radius of the HSA surface R_{ef} [19]).

For the purposes of 2D validation and the verification of the mathematical model of heat transfer in a high-velocity flow around blunt axisymmetric bodies, the calculated and experimental data given in [18] were used. According to the graphical dependences of work [3], the following error estimate for the 2D calculation of the convective heat flux q_w can be made: 20–37%. Testing the numerical method for solving 2D Euler equations is based on the calculation and comparison of vector and scalar fields of gas-dynamic parameters, the estimation of the shock wave receding Δ, and the value of the radius of curvature of the shock wave R_s on the axis of symmetry for a sphere or cylinder [3,26]. This testing showed that the gas-dynamic characteristics error is 5%; the error in the retraction Δ and the curvature of the shock wave R_s is 9% and 8.5%, respectively.

A comparison between the proposed mathematical model, experiments, and calculations [6,27–29] was made for the geometric model HSA X-33 (geometric scaling factor is 0.0132), as well as for the model created by Lockheed Martin for the aircraft demonstrator X-33 single-stage-to-orbit (SSTO). The studies were carried out for different attack angles [26,30–32]. In addition, a comparison was made for the HSA X-33 model [33].

The following parameters of the air flowing onto the vehicle were used (Table 1).

Table 1. Main parameters of the oncoming flow.

Parameter	X-33	X-43
Mach number in the oncoming flow	M = 6	M = 7
Pressure in the flow	p = 1120 Pa	p =1410 Pa
Velocity in the oncoming stream	V = 945 m/s	V = 1807 m/s
Temperature in the flow	T = 62,1 K	T = 227 K
The composition of the gas flowing onto the body	Air	Air
Height from the Earth's surface	H = 25 km	H = 30 km

In the performed calculations, the impingement angle (from 0 to 40 degrees) of the oncoming airflow (angle of attack) was used.

In addition, in [24] (for the geometric model of HSA X-33), a comparison was made between the calculated data obtained using the LANCH USA code [1] and an approximate mathematical model.

The value of the relative root-mean-square error is 29%. Here, it is also noted that the relative root-mean-square error for the heat flux at the "wing edge" is 5.7%. Figures 1 and 2 show the distributions of the convective heat flux for the upper and lower parts of the X-33 aircraft, and Figures 3 and 4 presented for the X-43 type respectively.

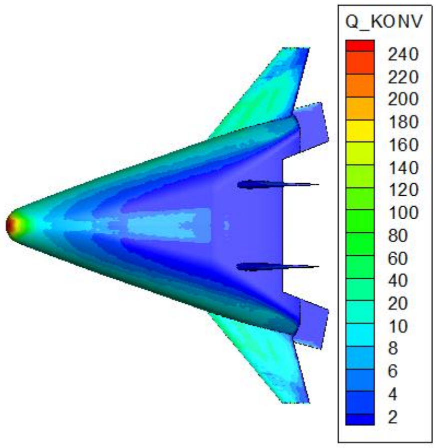

Figure 1. Convective heat distribution q_w (kW/m^2) for X-33 upper part, Mach number M = 6, height H = 25 km, attack angle α = 10°.

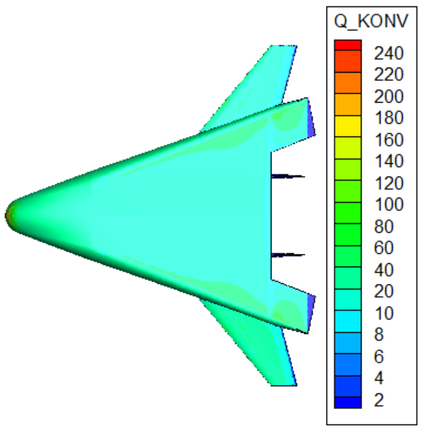

Figure 2. Distribution of convective heat flux q_w (kW/m^2) for the lower part of the X-33, Mach number M = 6, height H = 25 km, attack angle α = 10°.

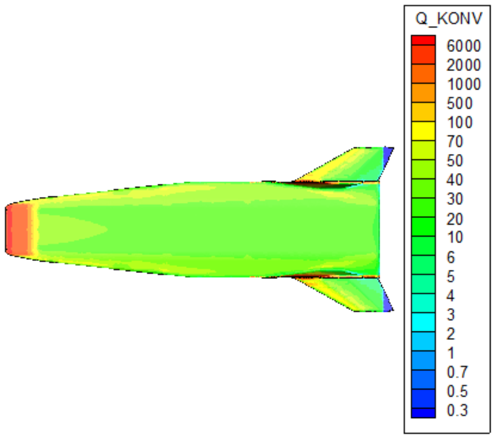

Figure 3. Convective flux q_w (kW/m^2) distribution for X-33 upper part, Mach number M = 6, height H = 25 km, attack angle α = 10°.

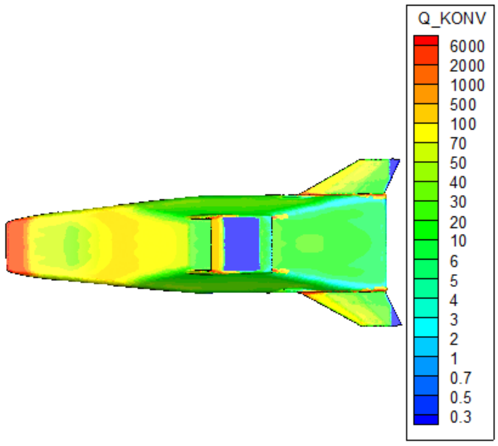

Figure 4. Distribution of convective heat flux q_w (kW/m^2) for the lower part of the X-43, Mach number M = 6, height H = 25 km, attack angle α = 10°.

In Table 2, the aerodynamic lift coefficients C_{ya}, drag forces C_{xa}, as well as the aerodynamic quality $K = C_{ya}/C_{xa}$ are shown for the X-33. Amendments have been introduced in the far right of the column which allows the evaluation of the accuracy of the performed calculations of the aerodynamic coefficients.

Table 2. Aerodynamic coefficients for the X-33 model.

Attack Angle	C_{ya} (Calc./Exp [10])	C_{ya} (Calc./Exp [10])	K	Comparison [%]
$\alpha = 0°$	0.3828	0.1173	3.26	
$\alpha = 20°$	0.3386/0.3102	0.2267/0.2539	1.49	10.7
$\alpha = 30°$	0.605/0.567	0.461/0.47	1.31	2
$\alpha = 40°$	0.798/0.76	0.7952/0.788	1.003	1

In Table 3 similar aerodynamic coefficients are presented for the X-43 vehicle.

Table 3. Aerodynamic coefficients for the X-43.

Attack Angle	C_{ya} (calc./Exp [11])	C_{ya} (Calc./Exp [11])	K	f.i. Comparison [%]
$\alpha = 0°$	0.2725	0.1223	2.23	
$\alpha = 2°$	0.3134/0.2985	0.1891/0.1775	1.65	6.1

Here, some discrepancies are noted (5–8%) in the aerodynamic coefficients (Tables 2 and 3) obtained using the above method, and the results of works [10,11] are mainly due to the approximation (in relation to the geometry of real devices) of the geometric models X-33 and X-43, as well as inaccuracies in the gas-dynamic calculation of the airflow around the external surfaces of these devices.

5. Conclusions

Of all the above problems, the following two were singled out and this work was devoted to these problems: the calculation of viscous shear stresses (and friction coefficient C_f) on the surface of a streamlined body, and the calculation of convective flow $q_{w,L}$ to the surface of a streamlined body.

The direct way to quickly estimate the friction coefficient and heat fluxes by numerically integrating the complete system of Navier–Stokes equations is problematic and is accompanied by serious difficulties and computer computing resources. This is because the characteristic size of the streamlined body (about ten meters) is much larger than the characteristic size of the boundary layer (boundary layer thickness: $\delta \approx 5 \cdot (\mu\ell/\rho U)^{0.5} \approx 1$ mm, where μ is the dynamic viscosity of the gas; ℓ is the characteristic length of the streamlined object; is the characteristic density of the gas; U is the characteristic velocity of the incoming flow), and the need to resolve the boundary layer near the surface of the streamlined body leads to the fact that the computational grid will require large amounts of random access memory and high-performance processors.

Therefore, one of the goals of the work was to develop a simplified (operational) method for estimating convective heat fluxes and drag coefficients for the bodies of simple and complex spatial shapes moving in the Earth's atmosphere. Thus, the method for assessing heat transfer near the HSA surface was formulated based on two physical and mathematical models: a 2D engineering–physical–mathematical model using bodies of simple geometric shapes, and a 3D numerical technique designed to calculate the complex geometric shapes of HSA using unstructured meshes [34].

An approximate mathematical model for calculating the friction coefficient and convective flux in the boundary layer [35–40] was built in this study. A novel computational method for the evaluation of the effective length effects was presented. Calculations based on the proposed mathematical model were carried out and compared with the experiments. Based on both experiments and calculations, the proposed mathematical model was Successful validation and verification of the proposed mathematical model was carried out on the basis of experiments and calculations carried out earlier. Successfully validated and verified. The heat flux q_w and the aerodynamic coefficients, C_{px} and C_{py}, are given for the geometric X-33 and X-43 models.

Author Contributions: Conceptualization, S.V.R. and A.Y.V.; software, V.V.K.; validation, V.V.K.; writing—original draft preparation, S.V.R. and V.V.K.; writing—review and editing, V.V.K., S.V.R. and A.Y.V.; project administration, S.V.R. All authors have read and agreed to the published version of the manuscript.

Funding: The results were obtained as part of the implementation of the Priority 2030 Program and the Federal Project of the Ministry of Science and Higher Education of the Russian Federation "Advanced Engineering Schools" (PISh).

Institutional Review Board Statement: Not applicable.

Informed Consent Statement: Not applicable.

Data Availability Statement: No new data were created or analyzed in this study. Data sharing does not apply to this article.

Conflicts of Interest: The authors declare no conflict of interest.

Nomenclature

C_a	Aerodynamic coefficient
C_f	Friction coefficient
C_p	Heat capacity (kJ/kg K)
$\vec{C_p}$	Pressure coefficient
F_f	Friction force
H	Height (m or km)
h	Heat transfer coefficient
$\mathrm{H_w}$	Enthalpy (J/kg)
HSA	High-speed aircraft
q	Convective heat flux (kW/m^2)
l_{eff}	Effective length
M	Mach number
m	Dimensionless velocity gradient
$\vec{n}$	Normal
P	Pressure (Pa)
Pr	Prandtl number
r	Temperature recovery factor
Re	Reynolds number
S	Surface area (m^2)
s	Streamline coordinate (m)
St	Stanton number
T	Temperature (K)
V	Velocity (m/s)
x	Abscissa
y	Ordinate
Greek symbols	
α	Angle of attack
δ	Thickness
ρ	Density (kg/m^3)
μ	Dynamic viscosity (Pa s)
τ_w	Frictional stress
γ	Adiabatic exponent
Π	Metric coefficient (m)
Δ	Error
0	Outer border
∞	Undisturbed gas
conv	Convective
L, lam	Laminar
mid	Midplane

References

1. Figliola, N.; Schmidt, D.; Lee, J.-H. Pressure-and Size-Dependent Aerodynamic Drag Effects on Mach 0. *3–2.2 Microspheres for High-Precision Micro-Ballistic Characterization. Appl. Sci.* **2022**, *12*, 6622. [CrossRef]
2. Wang, Z.; Hu, G.; Zhang, D.; Kim, B.; Xu, F.; Xiao, Y. Aerodynamic Characteristics of a Square Cylinder with Vertical-Axis Wind Turbines at Corners. *Appl. Sci.* **2022**, *12*, 3515. [CrossRef]
3. Ryzhkov, S.V.; Kuzenov, V.V. Analysis of the ideal gas flow over body of basic geometrical shape. *Int. J. Heat Mass Transf.* **2019**, *132*, 587–592. [CrossRef]
4. DeJarnette, F.; Hamilton, H.H.; Weilmuenster, K.J. New Method for Computing Convective Heating in Stagnation Region of Hypersonic Vehicles. In Proceedings of the 46 AIAA Aerospace Sciences Meeting and Exhibit, Aerospace Sciences Meetings, AIAA 2008–1261, Reno, NV, USA, 7–10 January 2008.
5. Ray, V.; Scheeres, D.J. Drag coefficient model to track variations due to attitude and orbital motion. *J. Guid. Control. Dyn.* **2020**, *43*, 1915–1926. [CrossRef]
6. Hollis, B.R.; Horvath, T.J.; Berry, S.A.; Hamilton, H.H.; Alter, S.J. X-33 Computational Aeroheating Predictions and Comparisons with Experimental Data. In Proceedings of the 33rd AIAA Thermophysics Conference, AIAA 99-3559, Norfolk, VA, USA, 28 June–1 July 1999.

7. Grigoryev, Y.N.; Vshivkov, V.A.; Fedoruk, M.P. *Numerical-Particle-in-Cell Methods*; Theory and Applications; Vandien Service Provider B.V.: Utrecht, The Netherlands, 2002.
8. Ramesh, R.; Morgan, R.G.; Mee, D.J. Heat Transfer Measurements in an Expansion Tube Using Infrared Thermography. *AIAA J.* **2022**, *60*, 883–891. [CrossRef]
9. Churakov, D.A.; Gorshkov, A.B.; Kovalev, R.V.; Dyadkin, A.A.; Zhurin, S.V. Heat Transfer of Reentry Vehicles during Atmosphere Flight. In Proceedings of the European Space Agency, ESA SP 659, Versailles, France, 3–6 November 2009.
10. Hollis, B.R.; Thompson, R.A.; Murphy, K.J.; Nowak, R.J.; Riley, C.J.; Wood, W.A.; Alter, S.J.; Prabhu, R. X-33 Aerodynamic and Aeroheating Computations for Wind Tunnel and Flight Conditions. In Proceedings of the 24th Atmospheric Flight Mechanics Conference, AIAA 99-4163, Portland, OR, USA, 9–11 August 1999.
11. Silvestrov, P.V.; Surzhikov, S.T. Calculation of aerothermodynamics for high-speed aircraft X-43 using computer code UST3D and UST3D-AUSMPW. *Phys. Chem. Kinet. Gas Dyn.* **2019**, *20*. Available online: http://doi.org/10.33257/PhChGD.20.4.865 (accessed on 4 September 2022). [CrossRef]
12. Kuzenov, V.V.; Ryzhkov, S.V. Numerical modeling of laser target compression in an external magnetic field. *Math. Model. Comput. Simul.* **2018**, *10*, 255–264. [CrossRef]
13. Surzhikov, S.T. Computing System for Solving Radiative Gasdynamic Problems of Entry and Re-Entry Space Vehicles. In Proceedings of the 1st International Workshop on Radiation of High Temperature Gases in Atmospheric Entry, ESA-533, Lisabon, Portugal, 8–10 October 2003; pp. 111–118.
14. Ryzhkov, S.V.; Kuzenov, V.V. New realization method for calculating convective heat transfer near the hypersonic aircraft surface. *Z. Für Angew. Math. Und Phys.* **2019**, *70*, 46. [CrossRef]
15. Vulis, L.A. *On the Overlap of Molecular and Molar Effects in the Transition Region of the Flow*; Gosenergoizdat: Moscow, Russia, 1963. (In Russian)
16. Gurvich, L.V.; Veits, I.V.; Medvedev, V.A.; Alcock, C.B. *Thermodynamic Properties of Individual Substances*; Nauka: Moscow, Russia, 1978; 495p. (In Russian)
17. Zinin, K.M.; Panasenko, A.V.; Surzhikov, S.T. Validation of computer code UST3D by the example of calculating the aerodynamic characteristics of the X-34 vehicle under various parameters. *Phys. Chem. Kinet. Gas Dyn.* **2019**, *20*. Available online: http://chemphys.edu.ru/media/published/Zinin_et_al_2019_Vol_20_No_4.pdf (accessed on 4 September 2022). [CrossRef]
18. Surzhikov, S.T. Calculation analysis of the experimental data of HIFiRE-1 using the computer code NERAT-2D. *J. Phys. Conf. Ser.* **2018**, *1009*, 012001. [CrossRef]
19. Shikin, E.V. Some questions of differential geometry in the large. *Am. Math. Soc. Transl. Ser.* **1996**, *2*, 176.
20. Andreev, S.V.; Bondarev, A.E.; Mikhailova, T.N.; Nesterenko, A.; Ryzhova, I. *Approximate Approach to Estimating Frictional Resistance on Bodies of Revolution in Viscous Flow*; Keldysh Institute Preprints: Moscow, Russia, 2014; Volume 102, p. 12. (In Russian)
21. Evans, J.S.; Schexnayder, C.J. Influence of chemical kinetics and unmixedness on burning in supersonic hydrogen flames. *AIAA J.* **1980**, *18*, 188–193. [CrossRef]
22. De Boor, C.A. *Practical Guide to Splines*; Springer: Berlin/Heidelberg, Germany, 1978.
23. Zoby, E.V.; Moss, J.N.; Sutton, K. Approximate convective heating analysis for hypersonic flows. *J. Spacecr. Rocket.* **1981**, *18*, 64–70. [CrossRef]
24. Hamilton, H.H.; Weilmuenster, K.J.; DeJarnette, F. Improved Approximate Method for Computing Convective Heating on Hypersonic Vehicles Using Unstructured Grids. In Proceedings of the 9th AIAA/ASME Joint Thermophysics and Heat Transfer Conference AIAA, San Francisco, CA, USA, 5–8 June 2006; p. 3394.
25. Hamilton, H.H.; Weilmuenster, K.J.; DeJarnette, F. Approximate Method for Computing Laminar and Turbulent Convective Heating on Hypersonic Vehicles Using Unstructured Grids. In Proceedings of the 41st AIAA Thermophysics Conference, San Antonio, TX, USA, 22–25 June 2009.
26. Kuzenov, V.V.; Ryzhkov, S.V. Approximate method for calculating convective heat flux on the surface of bodies of simple geometric shapes. *J. Phys. Conf. Ser.* **2017**, *815*, 012024. [CrossRef]
27. Martin, J.; Gliffs, N.J. *Atmospheric Reentry. An Introduction to Its Science and Engineering*; Prentice-Hall Inc.: Englewood, CO, USA, 1969.
28. Fay, J.A.; Riddell, F.R. Theory of stagnation point heat transfer in dissociated air. *J. Aeronaut. Sci.* **1958**, *25*, 73–85. [CrossRef]
29. Hollis, B.R.; Horvath, T.J.; Berry, S.A.; Hamilton, H.H.; Thompson, R.A.; Alter, S.J. X-33 Computational Aeroheating Predictions and comparison with experimental data. *J. Spacecraft Rockets* **2001**, *38*, 658–669. [CrossRef]
30. Kuzenov, V.V.; Ryzhkov, S.V. Approximate calculation of convective heat transfer near hypersonic aircraft surface. *J. Enhanc. Heat Transf.* **2018**, *25*, 181–193. [CrossRef]
31. Varaksin, A.Yu. Air tornado-like vortices: Mathematical modelling. *High Temp.* **2017**, *55*, 286–309. [CrossRef]
32. Varaksin, A.Yu.; Romash, M.E.; Kopeitsev, V.N.; Gorbachev, M.A. Method of impact on free nonstationary air vortices. *High Temp.* **2012**, *50*, 496–500. [CrossRef]
33. Tauber, M.E.; Sutton, K. Stagnation-point radiative heating relations for earth and mars entries. *J. Spacer.* **1991**, *28*, 40–42. [CrossRef]
34. Kuzenov, V.V.; Ryzhkov, S.V.; Varaksin, A.Y. The Adaptive Composite Block-Structured Grid Calculation of the Gas-Dynamic Characteristics of an Aircraft Moving in a Gas Environment. *Mathematics* **2022**, *10*, 2130. [CrossRef]
35. Varaksin, A.Yu. Two-phase boundary layer of gas with solid particles. *High Temp.* **2020**, *58*, 716–732. [CrossRef]

36. Bykov, L.V.; Molchanov, A.M.; Yanyshev, D.S.; Platonov, I.M. Modern approaches for calculating flow parameters during a laminar–turbulent transition in a boundary layer. *High Temp.* **2018**, *56*, 109–123. [CrossRef]
37. Formalev, V.F.; Kolesnik, S.A.; Garibyan, B.A. Analytical solution of the problem of conjugate heat transfer between a gasdynamic boundary layer and anisotropic strip. *Her. Bauman Moscow State Techn. Univ. Ser. Nat. Sci.* **2020**, *5*, 44–59. [CrossRef]
38. Khan, S.; Selim, M.M.; Khan, A.; Ullah, A.; Abdeljawad, T.; Ikramullah; Ayaz, M.; Mashwani, W.K. On the analysis of the non-newtonian fluid flow past a stretching/shrinking permeable surface with heat and mass transfer. *Coatings* **2021**, *11*, 566. [CrossRef]
39. Varaksin, A.Y.; Ryzhkov, S.V. Vortex Flows with Particles and Droplets (A Review). *Symmetry* **2022**, *14*, 2016. [CrossRef]
40. Arifeen, S.U.; Haq, S.; Ghafoor, A.; Ullah, A.; Kumam, P.; Chaipanya, P. Numerical solutions of higher order boundary value problems via wavelet approach. *Adv. Differ. Equ.* **2021**, *2021*, 347. [CrossRef]